Complex Radiation Impedance of Microstrip-Excited Magnetostatic-Surface Waves

ACHINTYA K. GANGULY, DENIS C. WEBB, MEMBER, IEEE, AND CRAWFORD BANKS

Abstract—**A technique is described for computing the radiation reactance of microstrip-excited MSSW's from a Hilbert transform of a previously derived expression of the radiation resistance. The series combination of the radiation reactance, radiation resistance, and an inductive reactance corresponding to a shorted section of microstrip line forms an equivalent circuit characterizing the excitation process. Supporting impedance measurements are presented and limitations of the model are discussed.**

I. Introduction

THE CHARACTERIZATION of the complex radiation impedance in terms of geometrical and material parameters is essential for the effective design and development of useful magnetostatic-surface-wave (MSSW) devices. In a previous paper [1], an expression for the radiation resistance R_m per unit length of an infinitely long YIG-loaded microstrip transmission line was obtained. R_m was then related to the real part of the input impedance of the most commonly used excitation geometry, a shorted transmission line. Unfortunately, the technique used to obtain R_m could not be directly employed to calculate the imaginary contribution to the radiation impedance X_m.

In this paper, we calculate X_m by taking a Hilbert transform of R_m, an approach used successfully by Nalamwar and Epstein [2] for surface-acoustic-wave excitation. Although R_m is expressed in a specific analytic form, it is in general so complex that it must be computed numerically. With very little extra computation, X_m may be obtained by the Hilbert transform method. From a knowledge of R_m, X_m, and the properties of the microstrip transmission line, a full equivalent circuit characterizing the excitation process can be derived.

Experimental results are presented in Section IV. Both real and imaginary portions of the radiation impedance are included for completeness. Because of their importance in realizing wideband operation, examples of a narrow microstrip width (0.05 mm) and a thick YIG film (10.5 μm) not evaluated in our previous study [1], are treated here. Finally, the comparison between experimental and theoretical results is discussed in Section V.

II. Equivalent Circuit Representation

The real part of the radiation resistance for the structure shown in Fig. 1 was determined by solving Maxwell's equations with appropriate boundary conditions at the various interfaces [1]. To avoid the excessive complexity of a full Maxwell equation approach with mixed boundary conditions, the current carried by the microstrip line was approximated by a uniform surface current. The power carried away by the MSSW was related to the surface current by the complex Poynting theorem, resulting in an analytic form for the radiation resistance per unit length R_m of an infinitely long transmission line.

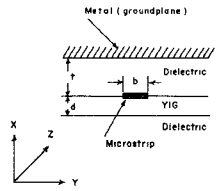

Fig. 1. Cross-sectional view of the excitation geometry. The magnetic bias lies along the $+Z$ direction.

The electromagnetic wave propagating along the transmission line is assumed to be of the form $\exp[-\alpha_0 z - i(\beta_0 z - \omega\tau)]$ where the attenuation α_0 is due entirely to energy carried away by the MSSW. For efficient MSSW excitation, the YIG-loaded section is terminated in a short circuit. If the transmission line has characteristic impedance Z_0', the input impedance to this shorted section is

$$Z_i = Z_0' \tanh(\alpha_0 + i\beta_0)l \tag{1}$$

where l is the line length from the short to the point of measurement. In the experiments described in this paper and, in fact, for most experimental conditions of interest, the approximations $\alpha_0 l \ll 1$ and $\beta_0 l \ll 1$ are valid. Re $[Z_i]$ then simplifies to the expression

$$R_i = \mathrm{Re}[Z_i] = R_m l/2. \tag{2}$$

Since the input impedance must be an analytic function of frequency, its real and imaginary parts are related by the Hilbert transforms [3]. Imaginary contributions which are linear in frequency can not be inferred from this argument, however, and must be deduced from physical reasoning. This is analogous to the surface-acoustic-wave input impedance determination in obtaining the static capacitive susceptance of the interdigital fingers [4]. In the present case, we note that, far from the frequency range of MSSW excitation, the input impedance must reduce to the usual value for a short section of shorted transmission line, i.e.,

$$Z_i \to i\omega Z_0 l/c$$

Manuscript received July 12, 1977; revised December 19, 1977.

The authors are with the Naval Research Laboratory, Washington, DC 20375.

where c is the electromagnetic wave velocity in the microstrip line and Z_0 is its charcteristic impedance. The full equivalent circuit thus consists of three series elements and is characterized by an input impedance of the form

$$Z_i = \frac{R_m l}{2} + i\frac{X_m l}{2} + i\omega\frac{Z_0 l}{c} \tag{3}$$

where X_m is the Hilbert transform of R_m.

III. Radiation Reactance

The radiation resistance R_m was shown to be given by the expression [1]

$$R_m = (A_+ + A_-)/2 \tag{4}$$

where

$$A_\pm = \mu_0 \omega R_{k0}^2 \left| \frac{\sin(bk_0/2)}{(bk_0/2)} \right|^2 \left[2k_0 d \{ (\mu_{12}s+1)^2 - \mu_{11}^2 \} \right]^{-2}$$
$$\cdot \left[2\frac{1 - 4k_0 t \exp(-2k_0 t) - \exp(-4k_0 t)}{[1+\exp(-2k_0 t)]^2} \right.$$
$$\cdot \{ (\mu_{12}s+1)\sinh(k_0 d) + \mu_{11}\cosh(k_0 d) \}^2$$
$$+ (\mu_{12}s + 2\mu_{11}k_0 d)\{ (\mu_{12}s+1)^2 - \mu_{11}^2 \}$$
$$- \{ \mu_{12}s[(\mu_{12}s+1)^2 - \mu_{11}^2] - 2\mu_{11}^2 \} \cosh(2k_0 d)$$
$$\left. - \mu_{11}(\mu_{12}^2 - 1 - \mu_{11}^2)\sinh(2k_0 d) \right]$$

$$R_{k0} = (\mu_{11} - \mu_{12}s - 1)\exp(-k_0 d)\tanh k_0 t$$
$$/A_{k0}(\mu_{11} - \mu_{12}s + \tanh k_0 t)$$
$$A_{k0} = 1 + \mu_{11}(t/d)(1 - \tanh^2 k_0 t)$$
$$\cdot [\mu_{11}^2 - (\mu_{12}s - \tanh k_0 t)^2]^{-1}. \tag{5}$$

ω and the wavenumber k_0 are related by the dispersion equation

$$\exp 2|k_0 d| = \frac{(\mu_{11} - \mu_{12}s - 1)(\mu_{11} + \mu_{12}s - \tanh|k_0|t)}{(\mu_{11} + \mu_{12}s + 1)(\mu_{11} - \mu_{12}s + \tanh|k_0|t)}. \tag{6}$$

In the above expressions, μ_{11} and μ_{12} are diagonal and off-diagonal components of the permeability tensor, respectively. $s = \pm 1$ and the dimensional quantities b, t, and d are defined in Fig. 1. Magnetic damping and anisotropy have not been included in these expressions.

X_m, the Hilbert transform of R_m, is given by the relation

$$X_m(\omega) = \frac{1}{\pi} P \int_{-\infty}^{+\infty} \frac{R_m(\omega')}{\omega' - \omega}\, d\omega' \tag{7}$$

where P denotes the principal value of the integral. Using the condition

$$P\int_{-\infty}^{+\infty} \frac{d\omega'}{\omega' - \omega} = 0 \tag{8}$$

the singularity in (7) may be removed and $X_m(\omega)$ expressed as

$$X_m(\omega) = \frac{1}{\pi}\int_{-\infty}^{+\infty} \frac{R_m(\omega') - R_m(\omega)}{\omega' - \omega}\, d\omega'. \tag{9}$$

Magnetostatic-surface waves on an infinite plane surface exist within a frequency range having a lower limit ω_1 given by

$$\omega_1 = \gamma[(H_i + 4\pi M)H_i]^{1/2} \tag{10}$$

and an upper limit ω_2 which depends on the state of metallization of the magnetic surface

$$\omega_2 = \gamma(H_i + 2\pi M), \quad \text{if unmetallized}$$
$$\omega_2 = \gamma(H_i + 4\pi M), \quad \text{if metallized.} \tag{11}$$

In the above expressions, γ is the gyromagnetic ratio, H_i is the dc magnetic field within the medium, and M is the saturation magnetization. If there is a dielectric medium between the metal and the magnetic film, then ω_2 lies between the two values given by (11). The exact value depends on the relative thicknesses of the dielectric and the magnetic media. The expression for $R_m(\omega)$ applies in the frequency range $\omega_1 < \omega < \omega_2$. We assume that

$$R_m(\omega) = 0, \quad \text{for } \omega < \omega_1 \text{ and } \omega > \omega_2.$$

From (4) and (5) we may also write $R_m(-\omega) = R_m(\omega)$, since changing the sign of ω is equivalent to reversing the direction of propagation. This merely interchanges the roles of the two terms A_+ and A_-. Using these properties of $R_m(\omega)$, (9) may be transformed into

$$X_m(\omega) = \frac{R_m(\omega)}{\pi}\ln\left[\frac{(1-\omega/\omega_2)\left(\frac{\omega}{\omega_1}+1\right)}{(1+\omega/\omega_2)\left(\frac{\omega}{\omega_1}-1\right)}\right] + \frac{2\omega}{\pi\omega_1}\int_1^{\omega_2/\omega_1} \frac{R_m(x\omega_1) - R_m(\omega)}{x^2 - (\omega/\omega_1)^2}\, dx. \tag{12}$$

Thus the imaginary part of the radiation impedance is obtained from (12) by a simple numerical integration.

IV. Results

Calculated curves for the radiation reactance and corresponding radiation resistance of the shorted microstrip transmission line are shown in Figs. 2 and 3 (solid curves). The YIG film is assumed to be placed on top of the microstrip (configuration A of [1]). Two samples approximately 2 mm wide ($l = 2$ mm) having YIG film thicknesses of 6.2 and 10.5 μm, respectively, were studied using two different microstrip exciters. The two microstrip lines consisted of 0.18- and 0.05-mm wide strips, respectively, on 0.25-mm thick alumina substrates. A magnetic field of 740 Oe was chosen to set the optimum excitation frequency at about 4 GHz.

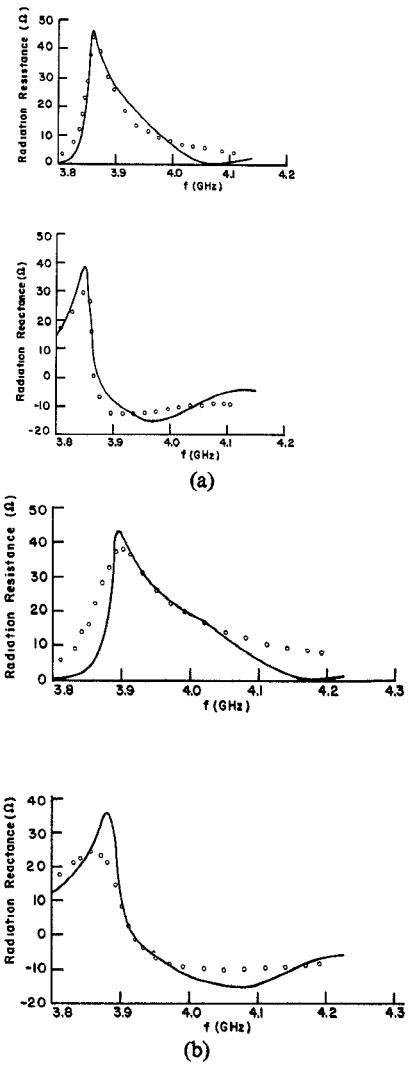

Fig. 2. Measured (circles) and computed MSSW radiation resistance $(R_m l/2)$ and reactance $(X_m l/2)$ for a shorted microstrip line. (a) $b=0.18$ mm, $d=6.2$ μm. (b) $b=0.18$ mm, $d=10.5$ μm.

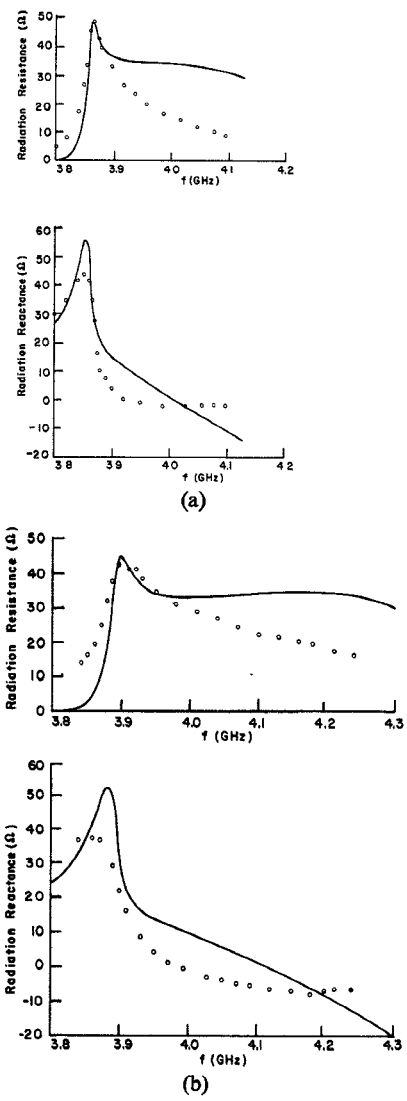

Fig. 3. Measured (circles) and computed MSSW radiation resistance $(R_m l/2)$ and reactance $(X_m l/2)$ for a shorted microstrip line. (a) $b=0.05$ mm, $d=6.3$ μm. (b) $b=0.05$ mm, $d=10.5$ μm.

The experimental points (circles) in Figs. 2 and 3 were obtained using a Hewlett-Packard 8545 automatic network analyzer as described in [1]. Time-domain reflectometer measurements were used again to accurately determine the reference plane (front edge of the sample) for the input impedance. The complex radiation impedance $(R_m l/2)+i(X_m l/2)$ was found by taking the difference $Z_i(H\neq 0)-Z_i(H=0)$. Because the crystallographic orientation of the samples is not known, the frequency of maximum radiation resistance of the experiment and theory were set to coincide; no other parameter was adjusted.

The best overall agreement between theory and experiment is seen to occur for excitation with the wide strip where all essential features of the response—amplitude, bandwidth, and shape—are well predicted by the model. Agreement is considerably poorer for the narrow strip case. Although the maximum value of radiation resistance is accurately predicted by the theory and an expected increase in bandwidth with decreasing strip width is observed, the measured bandwidth is considerably smaller than anticipated. Furthermore, the discrepancy in the shape of R_m causes a large corresponding discrepancy in X_m because of their transform relationship.

A likely major source of error is the assumption of a uniform current distribution in the microstrip line. If a more realistic current distribution, $I=I_0[1-(2y/b)]^{1/2}$ is assumed, the factor sin $(bk/2)$ in (5) is replaced by $J_0(bk/2)$ where J_0 is the Bessel function of order zero. Although not completely accounting for the narrow strip excitation behavior, it does have the effect of reducing the bandwidth of R_m by 20 percent without altering its maximum value. Further improvement in the agreement might be expected with a more accurate current distribution. Other assumptions in the model, e.g., $\alpha_0 l$, $\beta_0 l \ll 1$, no conductive losses, no energy stored in volume waves, and plane MSSW propagation, could introduce additional errors.

V. Conclusions

With certain simplifying assumptions, it has been shown that a meaningful three-series element equivalent

circuit representation of MSSW excitation can be obtained without resorting to the computational complexity of a full Maxwell equation—boundary value problem approach. Although the radiation resistance is a complicated function, it is of analytic form and thus is readily evaluated for a wide range of experimental conditions. The radiation reactance can be obtained from a numerical Hilbert transform of the resistance with little extra computational effort. Finally, the third element of the model can be derived from the characteristic impedance and guide wavelength of the microstrip line in the absence of MSSW excitation.

It is, unfortunately, not possible to draw a set of universal curves showing the dependence of Z_m on the various geometrical and material parameters. In this paper we have shown only those curves relevant to our experimental parameters to demonstrate the validity of the model; in general, Z_m must be calculated for each set of parameters of interest. However, from (4), (5), (6), and (9) it can be seen that, for a given bias field, $Z_m(\omega)$ does not change if the microstrip width b, dielectric thickness t, and magnetic layer thickness d are simultaneously scaled by a constant factor.

The experiments show that the equivalent circuit model is most effective for relatively wide stripwidths, but it accurately predicts the peak radiation resistance in all cases examined. For narrow strips, the correct qualitative dependence upon geometrical parameters is observed, but the bandwidth of the radiation resistance is consistently overestimated. The radiation reactance therefore also differs significantly from the predicted response. Despite these limitations, we believe the model to be a useful guide in the design of MSSW devices, both in selecting optimum geometrical parameters for the desired application and in designing appropriate matching circuitry.

Acknowledgment

The authors are indebted to A. Braginski of the Westinghouse Research Laboratories and H. Glass of the Electronics Research Division of Rockwell International for providing the YIG samples.

References

[1] A. K. Ganguly and D. C. Webb, "Microstrip excitation of magnetostatic surface waves: Theory and experiment," *IEEE Trans. Microwave Theory Tech.*, vol. MTT-23, pp. 998–1006, Dec. 1975.

[2] A. L. Nalamwar and M. Epstein, "Immittance characterization of acoustic surface-wave transducers," *Proc. IEEE*, vol. 60, pp. 336–337, Mar. 1972.

[3] E. A. Guillemin, *The Mathematics of Circuit Analysis*. New York: Wiley, 1949, pp. 330–349.

[4] R. F. Mitchell and N. H. C. Reilly, "Equivalence of δ-function and equivalent circuit models for interdigital acoustic-surface-wave transducers," *Electron. Lett.*, vol. 8, no. 13, pp. 329–330, June 1972.

Harmonic Analysis of SAW Transducers

CARL M. PANASIK AND BILL J. HUNSINGER

***Abstract*—The excitation function of an unapodized interdigital transducer (IDT) is determined by measuring the discrete impulse response, taking into account the first seven harmonics of the frequency domain. Using a time-segregation method, all non-SAW time-domain components are suppressed. A single transducer is isolated by a method of autodeconvolution that utilizes a theoretically derived phase function. The resulting excitation function provides experimental insight into the operation of IDT electrodes and compares well with the theoretical response of Smith and Pedler [3]. The basic analysis technique can be used for other configurations, once the frequency-domain phase response of one transducer is known.**

I. Introduction

AN EXPERIMENTAL analysis technique has been devised which produces the time-domain excitation function of an isolated interdigital transducer (IDT). The time-domain excitation function is defined as the instantaneous surface acoustic wave (SAW) amplitude displacement distribution resulting from a voltage impulse applied to the transducer. Works of Engan [1], Hartmann and Secrest [2], Smith and Pedler [3], Bahr and Lee [4], and Szabo *et al.* [5] have presented theoretical descriptions of the SAW electric fields produced by the IDT.

This paper describes a technique for measuring the SAW amplitudes produced by these driving source fields. The time-domain excitation function is found by measuring the transducer frequency-domain voltage transfer ratio in a low impedance system and transforming it to produce the time-domain SAW amplitude distribution resulting from the driving source fields.

Manuscript received July 12, 1977; revised February 2, 1978. This work was supported by the Air Force Avionics Laboratory under Contract F33615-75-R-1291 and by JSEP under Contract DAASB-07-72-C-0259.

The authors are with the College of Engineering, University of Illinois at Urbana–Champaign, Urbana, IL 61801.

II. Sampled Time-Domain Calculations

The frequency-domain transfer ratio is measured for the distinct purpose of being transformed to the time domain. The frequencies at which the transfer functions